THE JOURNAL OF PHYSICAL CHEMISTRY LETTERS
A JOURNAL OF THE AMERICAN CHEMICAL SOCIETY

pubs.acs.org/JPCL

Letter

Enhanced Mobility during Diels–Alder Reaction: Results of Molecular Simulations

Korey M. Reid and David M. Leitner*

Cite This: *J. Phys. Chem. Lett.* 2022, 13, 3763–3769

Read Online

ACCESS | Metrics & More | Article Recommendations | Supporting Information

ABSTRACT: Recent measurements indicate enhanced mobility of solvent molecules during Diels–Alder (DA) and other common chemical reactions. We present results of molecular dynamics simulations of the last stages of the DA cycloaddition reaction, from the transition state configuration to product, of furfurylamine and maleimide in acetonitrile at reactant concentrations studied experimentally. We find enhanced mobility of solvent and reactant molecules up to at least a nanometer from the DA product over hundreds of picoseconds. Local heating is ruled out as a factor in the enhanced mobility observed in the simulations, which is instead found to be due to solvent relaxation following the formation of the DA product.

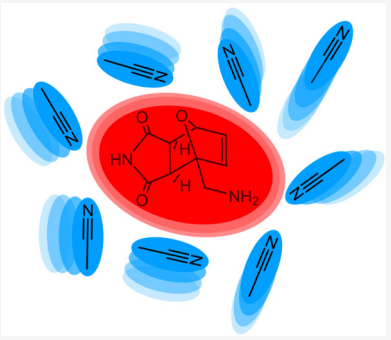

Numerous studies report enhancement of mobility of molecules during chemical reactions, with diffusion coefficients larger than those in the absence of the reaction.[1−10] Notable are reports of observation of boosted mobility of enzymes during enzyme-catalyzed reactions,[6−10] of which the origin remains unknown and efforts to clarify continue.[10−18] The enzyme-catalyzed reactions take place in dilute solution, so that collective effects of the reaction on other enzymes, such as, for example, collective thermal effects, can be ruled out.[16] Recently, Granick and co-workers have reported enhanced mobility during a number of common chemical reactions, including click reactions, ring-opening metathesis polymerization, and Sonogashira coupling, as well as a Diels–Alder (DA) reaction.[1] These reactions take place at a relatively high concentration. Some of the reactions have since been studied by others, who have noted little if any enhanced mobility,[19−22] although differences in conditions of experiments and measurements contribute to different observations.[23] The boosted mobility of solvent molecules during DA cycloaddition reactions was found to be less striking than that found for many of the other reactions and has not been subject to further experimental study to date. Motivated by the experimental work by Wang et al.,[1] we investigate the possibility of enhanced mobility during a DA cycloaddition reaction by molecular dynamics (MD) simulations. While the DA reactions exhibited a relatively small enhancement of mobility in the experiments, about 2–4%, the enhancement is statistically significant and the reaction step where at least much of the boost might occur, from the transition state configuration to product, can be modeled more readily than for other reactions.

We model by MD simulations the response of the DA product, reactants, and the solvent molecules during and following the final stage of the cycloaddition reaction, the transformation from the transition state configuration to product. The reaction studied experimentally, the cycloaddition of furfurylamine and maleimide, occurs in acetonitrile at a reactant concentration of about 100–300 mM, and we carry out MD simulations at about 210 mM reactant concentration. We examine the extent to which there is enhancement of mobility of the molecules in solution, specifically the acetonitrile solvent molecules, reactant molecules, and the DA product, in response to the DA reaction by comparing to the same system in the absence of reaction, and we explore the origin of any enhancement. We consider the possibility of local heating of the solution resulting from the reaction and the relaxation of solvent molecules in response to the reaction.

For the MD simulations, force field models for furfurylamine, maleimide, and the DA cycloaddition product were generated. The force fields are based on *ab initio* computational results with an implicit solvent (acetonitrile). The structure of the transition state (TS) was similarly computed and used to guide the displacement of the DA product toward the TS for initial structures in the simulations. Details of the *ab initio* computational work, carried out with Gaussian 16,[24] are

Received: March 27, 2022
Accepted: April 19, 2022

https://doi.org/10.1021/acs.jpclett.2c00886
J. Phys. Chem. Lett. 2022, 13, 3763–3769

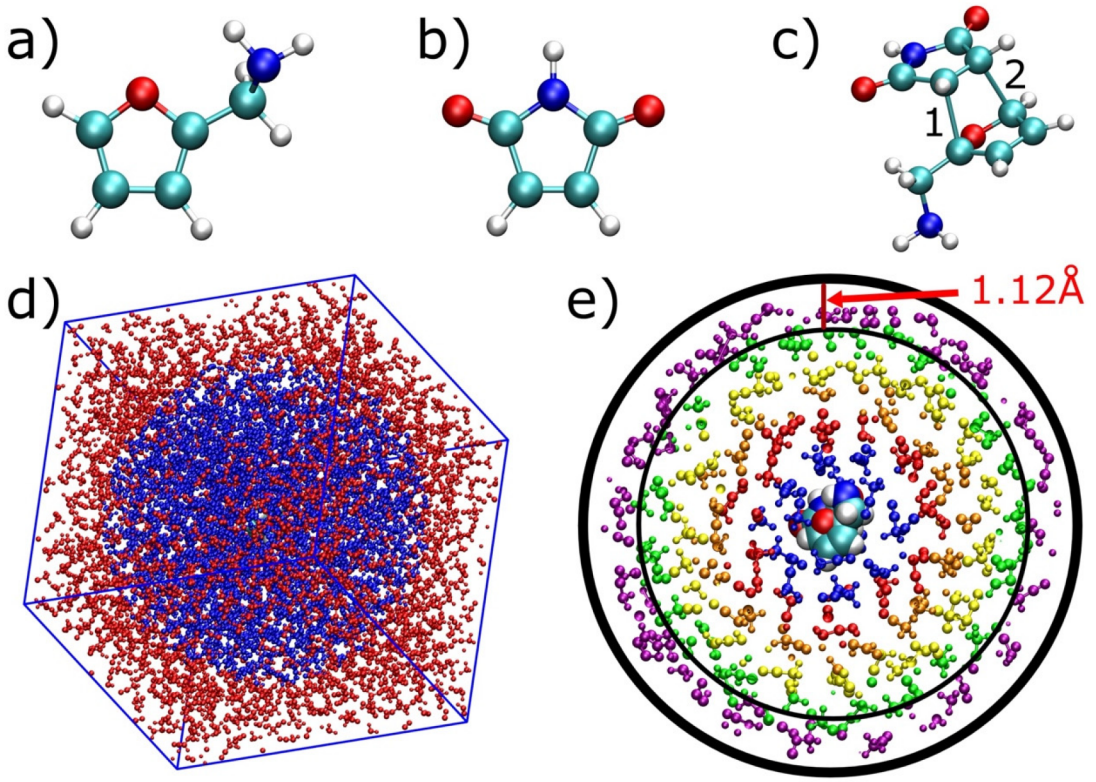

Figure 1. (a) Furfurylamine, (b) maleimide, and (c) exo Diels–Alder (DA) product. The bonds deformed to model the formation of product from the TS configuration labeled as 1 and 2 in panel c and the displacements given in Table 1. (d) Depiction of atoms within the box where red corresponds to the region with a thermostat and blue without a thermostat, where the diameter of the inner region is 90% of the average box length. Note that, for simulations solely under NVE integration, all atoms would be depicted as blue (not shown). (e) Depiction of spherical solvation shells of 1.12 Å width, each a different color, around the DA product.

presented in the Supporting Information. Structures of the reactants and the DA product are shown in Figure 1, and the bonds displaced for the TS structures are labeled as 1 and 2, with their displacement for two TS energies used in the MD simulations listed in Table 1. We will refer to these displacements as the TS configurations for the two initial states at energies of 1.1 and 1.5 eV in what follows. These are the energies released by the reaction in the MD simulations. We note that the activation volume that we have computed on the basis of Voronoi volumes of the TS configurations and the reactants is −65 Å^3 (see the Supporting Information for details), which is comparable to the value found for other DA cycloaddition reactions.[25,26]

Table 1. Potential Energy Difference between the TS Configuration at Two Different TS Energies and the Product Ground State (GS) Geometry[a]

$\Delta E_{TS^* \rightarrow product}$	bond 1 (Å)	bond 2 (Å)
−1.5 eV	1.82	1.79
−1.1 eV	1.80	1.78
GS	1.57	1.56

[a]Lengths of bonds 1 and 2 indicated in Figure 1c are different for the DA product and TS conformations.

Force field parameters for all of the molecules involved in the DA reaction were fit using the CHARMM force field[27] and the results of the *ab initio* computation. The full set of force field parameters used in the MD simulations are listed in the Supporting Information, where details of the MD simulations also appear. Here, we provide a summary. Simulations were performed with Large-scale Atomic/Molecular Massively Parallel Simulator (LAMMPS).[28] Both constant volume, constant energy simulations with a fixed number of particles (NVE), and simulations with a thermostat (NVT) at the edge of the simulation cell were carried out at 210 mM reactant concentration and one DA cycloaddition molecule in the TS configuration at a temperature of 273 K. Simulations were also carried out for control systems at the same concentration of reactants but no reaction, i.e., a cell containing the same concentration of reactants and the DA molecule already in the product configuration. For each system, with initial excess energy of 1.1 or 1.5 eV, the simulations were run 100 times and the results were averaged. For those simulations where a thermostat was adopted, the thermostat was used only in the outer shell of the reaction cell, as depicted in Figure 1. In those cases, we report only the mobility of molecules outside the region of the thermostat. We have carried out simulations with a thermostat because the temperature of the cell rises following reaction for the NVE simulations, as shown and discussed below, which could contribute to enhanced mobility.

Each simulation box was created with 1955 acetonitrile molecules, 9 furfurylamine molecules, 9 maleimide molecules, and 1 DA product molecule, in either the product configuration or the TS configuration. The DA molecule was placed at the center of the simulation cell, which started as a cubic box with sides equal to 55.5 Å, and maleimide and furfurylamine were evenly distributed, followed by solvating the system with acetonitrile. The system was equilibrated using

https://doi.org/10.1021/acs.jpclett.2c00886
J. Phys. Chem. Lett. 2022, 13, 3763−3769

a NPT simulation. To control for the possibility of temperature increase during reaction, we employed a spherical cutoff, where, inside the cutoff, the simulation was performed under NVE integration and, outside the cutoff, the molecules were simulated under NVT integration with a Langevin thermostat and a temperature coupling constant of 2.25 ps. We chose this value to avoid artifacts of periodic boundary conditions, accounting for the speed of sound in acetonitrile and the size of the simulation box. Other values chosen did not change the relative enhancement of mobility or the duration of this effect (see the Supporting Information). The radius of this spherical cutoff was set to 0.45 or 90% of half of the average box length of each side, depicted in Figure 1d.

We consider first energy relaxation from the initial DA TS configuration as it forms a product and any change in the temperature of the system that may result from this process. In Figure 2, we plot the temperature of the system, where, at the initial time, the DA molecule is in the TS configuration with an energy of 1.1 eV. Results of the NVE and NVT simulations are plotted. We observe that energy relaxes rapidly, within a few picoseconds, toward equilibrium, which occurs both with and without a thermostat. However, there is a rise in the temperature of almost 3 K or about 1% for the NVE simulation, whereas for the NVT simulation, the temperature returns to the initial value. Even this small change in the temperature has the potential to impact the mobility of the molecules of the system, particularly because the viscosity of acetonitrile is quite sensitive to the temperature and we are investigating the possibility of a small enhancement of mobility as a result of the reaction. To avoid potential artifacts that may arise by heating the system, we present results for the mobility of acetonitrile molecules, the reactants, and the DA product for systems with a thermostat applied to the edge of the simulation cell. It should be noted that this entirely classical simulation might miss quantum mechanical effects that could slow the rate of energy relaxation of the DA product and cooling of the system following formation of the DA product.[29−33] However, for a condensed phase system, we do not expect a dramatic increase in the cooling time when accounting for quantum effects on thermalization of the DA product,[29] and the energy relaxation time for the DA product is typical of that of many sizable molecules in the condensed phase.[34−44]

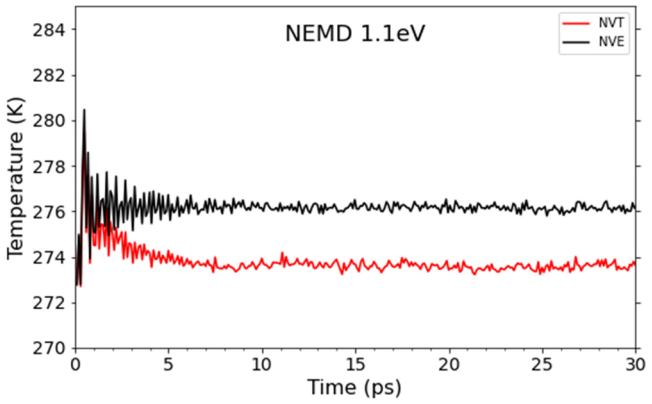

Figure 2. Thermal relaxation of the system during the transition from the TS configuration at 1.1 eV to the DA product as modeled by NVE (black) and NVT (red) simulations. The system returns to the original temperature in the NVT simulation but is heated by about 1% in the NVE simulation.

We examine mobility of acetonitrile, the reactants, and the DA product by computing the mean square displacement (MSD) from the initial positions based on the results of the MD simulations. The MSD of these molecules, averaged over 100 simulations, are plotted in Figure 3 for two energies for the TS, 1.1 and 1.5 eV. The MSD for the molecules in the systems undergoing reaction is compared to the MSD for the same molecules when no reaction occurs. At both energies, the MSD for acetonitrile appears very similar for the reactive simulations and is distinctly greater at any time than the MSD computed from the results of the non-reactive simulations. For the reactants, the MSD curves are also higher for the reactive simulations compared to those for the non-reactive simulations for both 1.1 and 1.5 eV initial energies over times to about 100 ps. Beyond 100 ps, they remain higher by about 10% than the results for the non-reactive simulations for the 1.5 eV reaction. For the DA product, the trends resemble those for the reactants.

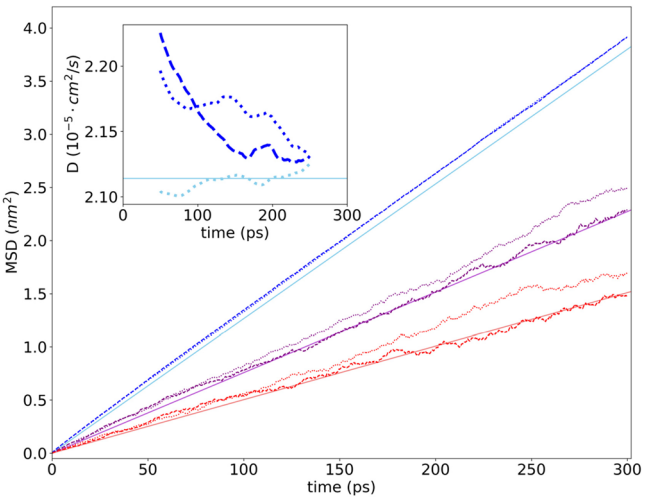

Figure 3. MSD versus time for acetonitrile (blue), reactants (purple), and the DA molecule (red). Solid lines correspond to MSD curves for non-reactive systems, where the average slope was taken from a least squares fit from 87.5 to 200 ps; each line starts at the origin and is color-matched to the non-equilibrium molecular dynamics (NEMD) results (cyan for acetonitrile). The inset corresponds to the diffusion coefficient, D, for acetonitrile for the reactions at 1.1 eV (dashed blue) and 1.5 eV (dotted blue), computed from a least squares fit to a 100 ps moving window. For reference, the value of D computed for the non-reactive system is plotted as a dotted curve (cyan) along with the value obtained from the linear fit to the MSD curve for the non-reactive system.

On the basis of the results plotted in Figure 3, the enhancement in mobility of the reactants and the DA product appears greater for the higher energy reaction than for the lower energy reaction. We note, however, that there are significantly more fluctuations in the data for the reactants and DA product compared to acetonitrile. There are 38 197 acetonitrile molecules outside the thermostat available for averaging in the 100 MD simulations that were run compared to 100 DA product molecules and 359 reactant molecules (see Figure S1 of the Supporting Information). This accounts for the much smoother data for acetonitrile, observed in Figure 3. The measurements of enhanced mobility during this reaction, as noted above, were made for the acetonitrile solvent.

https://doi.org/10.1021/acs.jpclett.2c00886
J. Phys. Chem. Lett. 2022, 13, 3763−3769

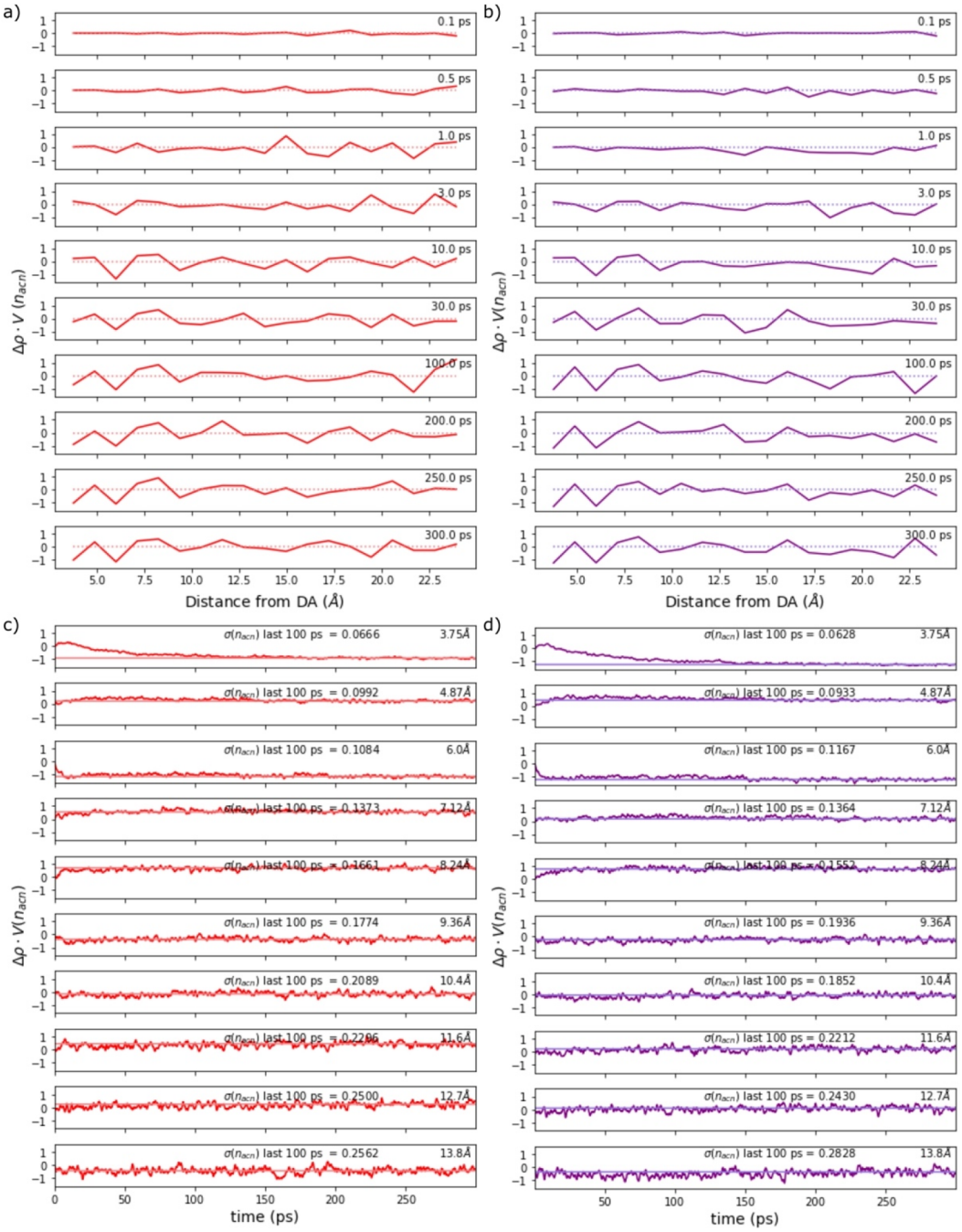

Figure 4. (a) 1.1 eV TS and (b) 1.5 eV TS are changes in the solvent number as a function of distance plotted at times from 0.1 to 300 ps following the reaction. (c) 1.1 eV TS and (d) 1.5 eV TS are changes with time in the solvent number in solvation shells out to about 14 Å from the DA product. A line fit to the last 100 ps of the 300 ps simulation is shown, so that the approach from earlier times can be better seen. The standard deviation in the change in the number of solvent molecules in the last 100 ps is indicated in panels c and d.

At both 1.1 and 1.5 eV, we see a larger MSD at any time for acetonitrile over the 300 ps plotted in comparison to the non-reactive system. Values for the diffusion coefficient, D, obtained from the slopes of the MSD curves for acetonitrile computed over running 100 ps intervals are presented for each system in the inset to Figure 3. There, we see that, at early times, to about 100−150 ps, D for acetonitrile is about 3% higher than for acetonitrile in the absence of the reaction. Over the next 100 ps, the value of D approaches the value when no reaction occurs, with the approach being somewhat faster for the lower energy, 1.1 eV reaction compared to the 1.5 eV energy change from the TS configuration to the product. By 300 ps, the values of D for the reactive and non-reactive systems become similar, although they remain somewhat higher still for the reactive system.

Enhanced mobility persists for several hundred picoseconds following completion of the reaction based on the results of the MD simulations. The time over which the DA product thermalizes and the system cools following the reaction is a few picoseconds (Figure 2), so that local heating during the reaction is not a factor. This conclusion is consistent with reports that exothermicity is not a requirement for boosted mobility.[1,45] Instead, we consider the response of the solvent to the reaction, specifically solvent density changes. The analysis

https://doi.org/10.1021/acs.jpclett.2c00886
J. Phys. Chem. Lett. 2022, 13, 3763−3769

that we carry out resembles earlier computational studies of water density fluctuations following ligand photolysis of myoglobin.[46] We examine the density changes in shells around the DA product, illustrated in Figure 1. The shells are of 1.12 Å thickness from the DA TS configuration as it evolves to the DA product. The results for the evolving density changes of acetonitrile in these shells are plotted in Figure 4.

In panels a and b of Figure 4, we plot at 10 specific times from the beginning of the reaction to 300 ps the change in the number of acetonitrile molecules in a given shell from its value at the initial time as a function of the distance from the DA molecule. The number is obtained from the local density and the volume of the spherical shell, and the distance that appears in Figure 4 is the distance between the center of mass of the DA product and the center of the shell. The 1.1 eV reaction is shown in Figure 4a, and the 1.5 eV reaction is shown in Figure 4b. We see at early times that the curves are flat, because the number of molecules in each shell has not yet changed in response to the reaction. However, at times of 1 ps and beyond, we observe changes of small amplitude at early times and larger amplitude later. Interestingly, adjustments in the number continue to appear over about 200 ps following completion of the reaction, even at distances quite far from the DA product.

In panels c and d of Figure 4, we plot for the 1.1 and 1.5 eV reactions, respectively, the change in the number of solvent molecules in each shell as a function of time to 300 ps. Looking at the shell closest to the DA product, we observe that the solvent number briefly rises and then becomes smaller, relaxing to about the final solvent number by about 200 ps. The initial rise corresponds to the change in configuration of the DA molecule from TS to the product, where the volume becomes smaller and solvent molecules move on average inward. As the solvent adjusts, the number of solvent molecules around the DA product again becomes smaller.

Upon examination of the direction of the velocity of solvent molecules surrounding the DA solute following the reaction, one finds that this dynamic is anisotropic. Solvent molecules along the direction of contraction of the DA molecule during the change from the TS configuration to the DA product move first toward the DA solute, within a few picoseconds, while there is a lag time, of about a picosecond, for those solvent molecules at a similar distance from the solute but at other orientations (see Figure S4 of the Supporting Information). At later times, the anisotropy becomes less apparent. By 20 ps, nearby solvent molecules generally move away from the solute, consistent with the dynamics observed in panels c and d of Figure 4. At longer times still, the directions become more randomized (see Figure S4 of the Supporting Information).

The trends are similar for both the lower and higher energy systems, although for the higher energy system, the adjustment in the number of solvent molecules in any shell takes somewhat longer to reach asymptotic values at long times. For both systems, moving even a nanometer beyond the DA molecule, we find the number of solvent molecules in the shell adjusts to the values at long times over at least 100 ps. Fluctuations in the change in the number of solvent molecules in a solvation shell, indicated in the panels c and d of Figure 4, increase with the distance of the shell from the DA molecule and are greater for the higher energy reaction than the lower energy reaction. Overall, on the basis of these results, we find the relaxation of the solvent following the reaction to occur over the same period of time as the enhancement of mobility of molecules involved in the reaction.

The results presented in Figure 4 indicate that, even on the 1 nm length scale, there are relaxation processes in the solvent that occur on time scales of 100 ps or beyond. This response is reminiscent of nanometer scale dynamic coupling between even modest sized biological molecules, such as small saccharides and solvent,[47,48] as well as much larger solutes, such as proteins and solvent[49−55] and DNA and solvent.[56] Computational modeling of dynamic coupling between the biomolecule and solvent typically found a smaller effect than that found by the experiment as a result of constraints on the size of the simulation cell.[49,50]

For the DA reaction modeled here, because of the size of the reaction cell used in the simulations and the need to introduce a thermostat at the edge of the reaction cell to avoid potential artifacts from heating the cell during reaction, a larger scale response to the reaction, beyond a roughly 1 nm radius from the DA molecule, remains a possibility. Even if the duration of the enhanced mobility observed in the MD simulations reported here is orders of magnitude shorter than the reaction rates in the experimental study, we cannot rule out the possibility of collective dynamics of solute and solvent beyond the reaction cell used in our simulations, which may further enhance mobility over longer times than those that we have found. Such long-range collective dynamics would be affected by the concentration of reactants, yielding concentration-dependent effects on the enhanced mobility, as observed experimentally.[1] Long-range effects of the reaction on the solvent might be most conveniently studied using more coarse-grained simulations. It would also be of interest to examine other systems studied in ref 1, for which no enhanced mobility was observed, including the S_N1 and S_N2 reactions, to see if such a null effect is also found in the simulations.

In conclusion, we have presented results of MD simulations of the last stages of the DA cycloaddition reaction of furfurylamine and maleimide in acetonitrile, starting from the TS configuration, at reactant concentrations studied in recent experiments. We find enhanced mobility of acetonitrile solvent molecules and reactant molecules up to at least a nanometer from the DA product as well as the DA product itself over hundreds of picoseconds. Local heating during the transition from the TS configuration to the product is not a factor in the enhanced mobility observed in the simulations, which is instead due to solvent relaxation following the formation of the DA product.

■ ASSOCIATED CONTENT

Supporting Information

The Supporting Information is available free of charge at https://pubs.acs.org/doi/10.1021/acs.jpclett.2c00886.

Ab initio computation and force field parameterization, simulation protocol, number of molecules in the inside and outside regions of the thermostat, local density following the reaction for different thermostats, computation of molecular volumes, solvent velocity profile, and force field parameters (PDF)

https://doi.org/10.1021/acs.jpclett.2c00886
J. Phys. Chem. Lett. 2022, 13, 3763−3769

AUTHOR INFORMATION

Corresponding Author

David M. Leitner − *Department of Chemistry, University of Nevada, Reno, Nevada 89557, United States;* orcid.org/0000-0002-3105-818X; Email: dml@unr.edu

Author

Korey M. Reid − *Department of Chemistry, University of Nevada, Reno, Nevada 89557, United States*

Complete contact information is available at: https://pubs.acs.org/10.1021/acs.jpclett.2c00886

Notes

The authors declare no competing financial interest.

ACKNOWLEDGMENTS

The authors thank Steve Granick, Martin Gruebele, and Huan Wang for numerous discussions from which this work emerged and benefitted. Support from National Science Foundation (NSF) Grant CHE-1854271 is gratefully acknowledged.

REFERENCES

(1) Wang, H.; Park, M.; Dong, R.; Kim, J.; Cho, Y.-K.; Tlusty, T.; Granick, S. Boosted Molecular Mobility during Common Chemical Reactions. *Science* **2020**, *369*, 537−541.

(2) Wang, H.; Huang, T.; Granick, S. Using NMR to Test Molecular Mobility during a Chemical Reaction. *J. Phys. Chem. Lett.* **2021**, *12*, 2370−2375.

(3) Jee, A.-Y.; Chen, K.; Tlusty, T.; Zhao, J.; Granick, S. Enhanced Diffusion and Oligomeric Enzyme Dissociation. *J. Am. Chem. Soc.* **2019**, *141*, 20062−20068.

(4) Huang, T.; Li, B.; Wang, H.; Granick, S. Molecules, the Ultimate Nanomotor: Linking Chemical Reaction Intermediates to Their Molecular Diffusivity. *ACS Nano* **2021**, *15*, 14947−14953.

(5) Xu, M.; Ross, J. L.; Valdez, L.; Sen, A. Direct Single Molecule Imaging of Enhanced Enzyme Diffusion. *Phys. Rev. Lett.* **2019**, *123*, 128101.

(6) Jee, A.-Y.; Tlusty, T.; Granick, S. Master Curve of Boosted Diffusion for 10 Catalytic Enzymes. *Proc. Natl. Acad. Sci. U. S. A.* **2020**, *117*, 29435−29441.

(7) Ghosh, S.; Somasundar, A.; Sen, A. Enzymes as Active Matter. *Annu. Rev. Cond. Matt. Phys.* **2021**, *12*, 177−200.

(8) Arqué, X.; Romero-Rivera, A.; Feixas, F.; Patiño, T.; Osuna, S.; Sánchez, S. Intrinsic Enzymatic Properties Modulate the Self-Propulsion of Micromotors. *Nat. Commun.* **2019**, *10*, 2826.

(9) Sengupta, S.; Dey, K. K.; Muddana, H. S.; Tabouillot, T.; Ibele, M. E.; Butler, P. J.; Sen, A. Enzyme Molecules as Nanomotors. *J. Am. Chem. Soc.* **2013**, *135*, 1406−1414.

(10) Jee, A.-Y.; Cho, Y.-K.; Granick, S.; Tlusty, T. Catalytic Enzymes Are Active Matter. *Proc. Natl. Acad. Sci. U. S. A.* **2018**, *115*, E10812−E10821.

(11) Bai, X.; Wolynes, P. G. On the Hydrodynamics of Swimming Enzymes. *J. Chem. Phys.* **2015**, *143*, 165101.

(12) Golestanian, R. Enhanced Diffusion of Enzymes That Catalyze Exothermic Reactions. *Phys. Rev. Lett.* **2015**, *115*, 108102.

(13) Agudo-Canalejo, J.; Adeleke-Larodo, T.; Illien, P.; Golestanian, R. Enhanced Diffusion and Chemotaxis at the Nanoscale. *Acc. Chem. Res.* **2018**, *51*, 2365−2372.

(14) Kondrat, S.; Popescu, M. N. Brownian Dynamics Assessment of Enhanced Diffusion Exhibited by 'Fluctuating Dumbbell Enzymes. *Phys. Chem. Chem. Phys.* **2019**, *21*, 18811−18815.

(15) Feng, M.; Gilson, M. K. A Thermodynamic Limit on the Role of Self-Propulsion in Enhanced Enzyme Diffusion. *Biophys. J.* **2019**, *116*, 1898−1906.

(16) Feng, M.; Gilson, M. K. Enhanced Diffusion and Chemotaxis of Enzymes. *Annu. Rev. Biophys.* **2020**, *49*, 87−105.

(17) Pressé, S. A Thermodynamic Perspective on Enhanced Enzyme Diffusion. *Proc. Natl. Acad. Sci. U. S. A.* **2020**, *117*, 32189−32191.

(18) Samanta, T.; Sarhangi, S. M.; Matyushov, D. V. Enhanced Molecular Diffusivity through Destructive Interference between Electrostatic and Osmotic Forces. *J. Phys. Chem. Lett.* **2021**, *12*, 6648−6653.

(19) Günther, J.-P.; Fillbrook, L. L.; MacDonald, T. S. C.; Majer, G.; Price, W. S.; Fischer, P.; Beves, J. E. Comment on "Boosted Molecular Mobility during Common Chemical Reactions". *Science* **2021**, *371*, eabe8322.

(20) Wang, H.; Park, M.; Dong, R.; Kim, J.; Cho, Y.-K.; Tlusty, T.; Granick, S. Response to Comment on "Boosted Molecular Mobility during Common Chemical Reactions". *Science* **2021**, *371*, eabe8678.

(21) Rezaei-Ghaleh, N.; Agudo-Canalejo, J.; Griesinger, C.; Golestanian, R. Molecular Diffusivity of Click Reaction Components: The Diffusion Enhancement Question. *J. Am. Chem. Soc.* **2022**, *144*, 1380−1388.

(22) Fillbrook, L. L.; Günther, J.-P.; Majer, G.; O'Leary, D. J.; Price, W. S.; VanRyswyk, H.; Fischer, P.; Beves, J. E. Following Molecular Mobility during Chemical Reactions: No Evidence for Active Propulsion. *J. Am. Chem. Soc.* **2021**, *143*, 20884−20890.

(23) Huang, T.; Wang, H.; Granick, S. Reply to Comment on "Using NMR to Test Molecular Mobility during a Chemical Reaction. *J. Phys. Chem. Lett.* **2021**, *12*, 5744−5747.

(24) Frisch, M. J.; Trucks, G. W.; Schlegel, H. B.; Scuseria, G. E.; Robb, M. A.; Cheeseman, J. R.; Scalmani, G.; Barone, V.; Petersson, G. A.; Nakatsuji, H.; Li, X.; Caricato, M.; Marenich, A.; Bloino, J.; Janesko, B. G.; Gomperts, R.; Mennucci, B.; Hratchian, H. P.; Ortiz, J. V.; Izmaylov, A. F.; Sonnenberg, J. L.; Williams-Young, D.; Ding, F.; Lipparini, F.; Egidi, F.; Goings, J.; Peng, B.; Petrone, A.; Henderson, T.; Ranasinghe, D.; Zakrzewski, V. G.; Gao, J.; Rega, N.; Zheng, G.; Liang, W.; Hada, M.; Ehara, M.; Toyota, K.; Fukuda, R.; Hasegawa, J.; Ishida, M.; Nakajima, T.; Honda, Y.; Kitao, O.; Nakai, H.; Vreven, T.; Throssell, K.; Montgomery, J. A., Jr.; Peralta, J. E.; Ogliaro, F.; Bearpark, M.; Heyd, J. J.; Brothers, E.; Kudin, K. N.; Staroverov, V. N.; Keith, T.; Kobayashi, R.; Normand, J.; Raghavachari, K.; Rendell, A.; Burant, J. C.; Iyengar, S. S.; Tomasi, J.; Cossi, M.; Millam, J. M.; Klene, M.; Adamo, C.; Cammi, R.; Ochterski, J. W.; Martin, R. L.; Morokuma, K.; Farkas, Ö.; Foresman, J. B.; Fox, D. J. *Gaussian 16, Revision 16*; Gaussian, Inc.: Wallingford, CT, 2016.

(25) Chen, B.; Hoffmann, R.; Cammi, R. The Effect of Pressure on Organic Reactions in Fluids—A New Theoretical Perspective. *Angew. Chem.* **2017**, *56*, 11126−11142.

(26) Kiselev, V. D.; Shakirova, I. I.; Kornilov, D. A.; Kashaeva, H. A.; Potapova, L. N.; Konovalov, A. I. Homo-Diels−Alder Reaction of a Very Inactive Diene, Bicyclo[2,2,1]hepta-2,5-diene, with the Most Active Dienophile, 4-Phenyl-1,2,4-Triazolin-3,5-Dione. Solvent, Temperature, and High Pressure Influence on the Reaction Rate. *J. Phys. Org. Chem.* **2013**, *26*, 47−53.

(27) Huang, J.; Rauscher, S.; Nawrocki, G.; Ran, T.; Feig, M.; deGroot, B. L.; Grubmuller, H.; MacKerell, A. D. Charmm36m: An Improved Force Field for Folded and Intrinsically Disordered Proteins. *Nat. Methods* **2017**, *14*, 71−73.

(28) Plimpton, S. Fast Parallel Algorithms for Short-Range Molecular Dynamics. *J. Comput. Chem.* **1995**, *117*, 1−19.

(29) Leitner, D. M. Quantum Ergodicity and Energy Flow in Molecules. *Adv. Phys.* **2015**, *64*, 445−517.

(30) Logan, D. E.; Wolynes, P. G. Quantum Localization and Energy Flow in Many-Dimensional Fermi Resonant Systems. *J. Chem. Phys.* **1990**, *93*, 4994−5012.

(31) Bigwood, R.; Gruebele, M.; Leitner, D. M.; Wolynes, P. G. The Vibrational Energy Flow Transition in Organic Molecules: Theory Meets Experiment. *Proc. Natl. Acad. Sci. U.S.A.* **1998**, *95*, 5960−5964.

(32) Gruebele, M. Molecular Vibrational Energy Flow: A State Space Approach. *Adv. Chem. Phys.* **2007**, *114*, 193−261.

(33) Keshavamurthy, S. Scaling Perspective on Intramolecular Vibrational Energy Flow: Analogies, Insights and Challenges. *Adv. Chem. Phys.* **2013**, *153*, 43−110.

(34) Pein, B. C.; Sun, Y.; Dlott, D. D. Controlling Vibrational Energy Flow in Liquid Alkylbenzenes. *j. Phys. Chem. B* **2013**, *117*, 10898−10904.
(35) Pein, B. C.; Dlott, D. D. Modifying Vibrational Energy Flow in Aromatic Molecules: Effects of Ortho Substitution. *J. Phys. Chem. A* **2014**, *118*, 965−973.
(36) Mizutani, Y.; Kitagawa, T. Direct Observation of Cooling of Heme Upon Photodissociation of Carbonmonoxy Myoglobin. *Science* **1997**, *278*, 443−446.
(37) Fujii, N.; Mizuno, M.; Mizutani, Y. Direct Observation of Vibrational Energy Flow in Cytochrome C. *J. Phys. Chem. B* **2011**, *115*, 13057−64.
(38) Leitner, D. M. Energy Flow in Proteins. *Annu. Rev. Phys. Chem.* **2008**, *59*, 233−259.
(39) *Proteins: Energy, Heat and Signal Flow*; Leitner, D. M., Straub, J. E., Eds.; CRC Press (Taylor & Francis Group): Boca Raton, FL, 2010.
(40) Botan, V.; Backus, E. H. G.; Pfister, R.; Moretto, A.; Crisma, M.; Toniolo, C.; Nguyen, P. H.; Stock, G.; Hamm, P. Energy Transport in Peptide Helices. *Proc. Natl. Acad. Sci. U. S. A.* **2007**, *104*, 12749−12754.
(41) Stock, G. Classical Simulation of Quantum Energy Flow in Biomolecules. *Phys. Rev. Lett.* **2009**, *102*, 118301.
(42) Maitra, A.; Sarkar, S.; Leitner, D. M.; Dawlaty, J. M. Electric Fields Influence Intramolcular Vibrational Energy Relaxation and Line Widths. *J. Phys. Chem. Lett.* **2021**, *12*, 7818−7825.
(43) Rodgers, J. M.; Zhang, W.; Bazewicz, C. G.; Chen, J.; Brewer, S. H.; Gai, F. Kinetic Isotope Effect Provides Insight into the Vibrational Relaxation Mechanism of Aromatic Molecules: Application to Cyano-Phenylalanine. *J. Phys. Chem. Lett.* **2016**, *7*, 1281−1287.
(44) Schmitz, A. J.; Pandey, H. D.; Chalyavi, F.; Shi, T.; Fenlon, E. F.; Brewer, S. H.; Leitner, D. M.; Tucker, M. J. Tuning Molecular Vibrational Energy Flow within an Aromatic Scaffold Via Anharmonic Coupling. *J. Phys. Chem. A* **2019**, *123*, 10571−10581.
(45) Illien, P.; Zhao, X.; Dey, K. K.; Butler, P. J.; Sen, A.; Golestanian, R. Exothermicity Is Not a Necessary Condition for Enhanced Diffusion of Enzymes. *Nano Lett.* **2017**, *17*, 4415−4420.
(46) Brinkmann, L. U. L.; Hub, J. S. Ultrafast Anisotropic Protein Quake Propagation after CO Photodissociation in Myoglobin. *Proc. Natl. Acad. Sci. U. S. A.* **2016**, *113*, 10565−10570.
(47) Heugen, U.; Schwaab, G.; Bründermann, E.; Heyden, M.; Yu, X.; Leitner, D. M.; Havenith, M. Solute-Induced Retardation of Water Dynamics Probed Directly by Terahertz Spectroscopy. *Proc. Natl. Acad. Sci. U. S. A.* **2006**, *103*, 12301−12306.
(48) Heyden, M.; Bründermann, E.; Heugen, U.; Niehues, G.; Leitner, D. M.; Havenith, M. Long-Range Influence of Carbohydrates on the Solvation Dynamics of Water: Answers from Terahertz Absorption Measurements and Molecular Modeling Simulations. *J. Am. Chem. Soc.* **2008**, *130*, 5773−5779.
(49) Ebbinghaus, S.; Kim, S. J.; Heyden, M.; Yu, X.; Heugen, U.; Gruebele, M.; Leitner, D. M.; Havenith, M. An Extended Dynamical Hydration Shell around Proteins. *Proc. Natl. Acad. Sci. U. S. A.* **2007**, *104*, 20749−20752.
(50) Leitner, D. M.; Gruebele, M.; Havenith, M. Solvation Dynamics of Biomolecules: Modeling and Terahertz Experiments. *HFSP Journal* **2008**, *2*, 314−323.
(51) Charkhesht, A.; Regmi, C. K.; Mitchell-Koch, K. R.; Cheng, S.; Vinh, N. Q. High-Precision Megahertz-to-Terahertz Dielectric Spectroscopy of Protein Collective Motions and Hydration Dynamics. *J. Phys. Chem. B* **2018**, *122*, 6341−6350.
(52) Heyden, M. Heterogeneity of Water Structure and Dynamics at the Protein-Water Interface. *J. Chem. Phys.* **2019**, *150*, 094701.
(53) Reid, K. M.; Singh, A. K.; Bikash, C. R.; Wei, J.; Tal-Gan, Y.; Vinh, N. Q.; Leitner, D. M. The Origin and Impact of Bound Water around Intrinsically Disordered Proteins. *Biophys. J.* **2022**, *121*, 540−551.
(54) Heyden, M.; Tobias, D. J.; Matyushov, D. V. Terahertz Absorption of Dilute Aqueous Solutions. *J. Chem. Phys.* **2012**, *137*, 235103.
(55) Martin, D. R.; Matyushov, D. V. Terahertz Absorption of Lysozyme in Solution. *J. Chem. Phys.* **2017**, *147*, 084502.
(56) Singh, A. K.; Wen, C.; Cheng, S.; Vinh, N. Q. Long-Range DNA−Water Interactions. *Biophys. J.* **2021**, *120*, 4966−4979.

https://doi.org/10.1021/acs.jpclett.2c00886
J. Phys. Chem. Lett. 2022, 13, 3763−3769